Characterization of Asian Tropospheric Aerosols with Multi-wavelength Mie-Raman Lidar and Skyradiometer

Toshiyuki Murayama*[a], Miho Sekiguchi[a], Detlef Müller[b], Katsuya Wada[a], and Yasuharu Saito[a]

[a]*Faculty of Marine Technology, 2-1-6 Etchujima, Koto, Tokyo 135-8533, Japan*
[b]*Institute for Tropospheric Research, Permoserstr. 15, 04318 Leipzig, Germany*

ABSTRACT

We have extensively observed tropospheric aerosols with lidar and Sun/sky radiometer in Tokyo. Recently, we have extended the lidar system to dual-wavelength Raman lidar (The primary laser wavelengths are 355 and 532 nm.). We found that the intensive optical properties such as Angstrom exponent and lidar ratios derived from the Raman lidar measurements are quite useful to characterize the aerosols resolving with height. As highlighted examples, we will show the case studies of Asian dust and Siberian smoke. For the smoke case (as spherical aerosol case), we retrieved the microphysical properties by applying an inversion with regularization. The results show an accumulation-mode dominate size-distribution and a low absorption; the effective radius and the single scattering albedo are ~0.22μm and ~0.95, respectively. The column-averaged microphysical properties derived from the skyradiometer are also consistent with the results. We also estimated the aerosol direct radiative forcing using the microphysical properties. Further systematic analyses and improvement of lidar system are now in progress.

Keywords: Raman lidar, Asian dust, Siberian forest-fire smoke, aerosol optical properties, aerosol radiative forcing

1. INTRODUCTION

Aerosols play an important role in the Earth's radiation budget through the scattering and absorption of light, and present a key uncertainty in the assessment of radiative forcing.[1] They also serve as cloud condensation nuclei and modulate the cloud properties. East Asia is considered as a region where emission of anthropogenic aerosol is rapidly increasing due to growing economy. Recently, the Asia-Pacific Regional Aerosol Characterization Experiment (ACE-Asia) showed that the spatial variability of aerosol composition and properties is rather high in this area.[2, 3] It is also shown that mineral dust has an indirect effect on clouds by serving as effective ice nuclei.[4-8] Therefore, it is highly important to study not only column-averaged but also height-resolved aerosol optical properties regularly, in order to assess their radiative impact. However, it is rather difficult to perform aircraft measurements frequently. Nowadays, sophisticated multi-wavelength Raman lidars enable us to characterize tropospheric aerosols by the observable quantities themselves, and in further to retrieve microphysical properties from them.[9-11] From the point of view of feasibility, we installed a UV-Raman lidar system that emits the third harmonic frequency (355 nm) on the basis of a second Nd:YAG laser in addition to our existed lidar system at the Etchujima campus (35.66° N, 139.80° E)of Tokyo University of Marine Science and Technology (TUMSAT).[12] Thus

* mrayama@e.kaiyodai.ac.jp; phone +81-3-5345-7464; fax +81-3-5245-7339

our lidar system is capable of measuring backscatter coefficients at 355, 532, 1064 nm, extinction coefficients at 355 and 532 nm, particle depolarization ratio at 532 nm, and water–vapor mixing ratio, simultaneously. To our knowledge, this is the first dual-wavelength Raman lidar installed in East Asia. In this paper, we demonstrate how the dual-wavelength Raman lidar is useful for the characterization of aerosol optical properties depending on regional aerosol events. We outline the Raman lidar system and the analysis method in section 2. In section 3, we presents results of observations for the case of Asian dust and Siberian forest-fire smoke events in the spring of 2003 with emphasis on the aerosol characterization by observed aerosol optical properties. In section 4, we present the microphysical parameters of the smoke derived from the inversion code, comparison with the results from the skyradiometer analysis, and an application for estimating the aerosol radiative forcing using these results. Most of the results presented here are described in the reference 13.

2. LIDAR SYSTEM AND ANALYTICAL PROCEDURE

We installed a UV-Raman lidar system next to the existing Mie-Polarization-Raman lidar, which uses the laser beams at 532 (VIS) and 1064 nm (IR)[3,12] The schematic view of the full lidar system is shown in Fig. 1. The UV-Raman lidar system is a stand-alone system, which employs another Q-switched Nd:YAG laser with a third harmonics generator. The repetition frequency of the laser pulse is 10 Hz, which is synchronized with the VIS/IR system. The receiving telescope is of Schmid-Cassegranian type with 35.5-cm diameter and the field of view is 2 mrad. The optical axes of the laser beams and the telescopes were well co-aligned each other in the vertically direction. These conditions allow us to observe nearly the same volume in time and space with both lidar systems. Dichroic mirrors and following narrow interference filters, which bandwidths are 1-3 nm, are used to separate the backscattered light from Mie-Rayleigh scattering (355 nm) and from Raman scattering from nitrogen (387 nm) and water-vapor molecules (408 nm). Similarly the Raman signals at 607 nm and the Mie/Rayleigh signals at 1064 nm were separated from the signals at 532 nm in the VIS/IR lidar system. Photo-multiplier tubes are used for the detection. The data were stored every 4094 shots (~7 minutes) using transient recorders (TR20-160, Licel). Typical laser powers during operation are approximately 100, 100, 200 mJ per pulse for the 355, 532 and 1064 nm laser beams. Lower height data evaluation were limited by the incomplete overlapping between the telescope field of view and the laser beams below ~1-1.5 km. Only the backscatter ratio at 355 nm and the water-vapor mixing ratio are evaluated almost down to the surface because we can regard the geometrical form factor as identical for both elastic and inelastic Raman channels. It is not the case for the backscatter ratio at 532 nm presented here because we used different receivers for the 532 nm and 607 nm signals. At this moment, the operation of Raman channels is limited in nighttime.

We have analyzed averaged or integrated analog and photon-counting data for observations lasting a few hours when the vertical structure did not vary significantly. The extinction coefficient and the scattering ratio of the aerosols at 355 and 532 nm, and the mixing ratio are derived by the methods given the references 14-16. The atmospheric density profile was calculated from routine radiosonde observations at Tateno (36.05° N, 140.12° E) at 12 UTC. Normalization of the scattering ratio is made at an almost aerosol-free height, typically over 10 km. The backscatter coefficients are derived from the backscatter ratios. The backscatter coefficient at 1064 nm is obtained from the Mie-Rayleigh signal by using the method proposed by Fernald[17] and assuming a lidar ratio of 40 sr. The lidar-derived water-vapor mixing ratio is normalized so that the lowest value (~75 m above the lidar) matches to the surface observation at TUMSAT with assuming the error of ±10 %. The mixing ratio profile was converted to the relative humidity one using the temperature and pressure profiles

obtained from the radiosonde data. Deviations of the mixing ratio and relative humidity obtained from the lidar at TUMSAT to the respective quantities derived with the radiosonde can be attributed to the spatial distance of the two sites and different measurement times, and the unknown error of the calibration factor of the lidar.

3. EXAMPLES OF OBSERVATION

3.1.Case of Asian dust

Fig. 2 presents the time-height cross-sections of the backscatter coefficient and total (particle + molecular) depolarization ratio at 532 nm on 12 March 2003. The depolarization ratio is an indicator of irregularly shaped particles. Fig. 3 shows the mean profiles for a measurement period from 1056 to 1306 UTC. We also indicated the Ångström exponent (AE) and the backscatter-related Ångström exponent (BAE) derived from the profiles of the extinction and backscatter coefficient at 355 and 532 nm, respectively. The error bars are based on statistical and estimated systematic errors. The aerosol layer between 3 and 5 km seems to be composed of two layers as indicated by the horizontal dashed lines A and B in Figure 2: layer A is rather narrow with the peak at 4.6 km, layer B is broader with the peak at 4.0 km. The lower layer B carries features of mineral dust as suggested from the high particle depolarization ratio (PDR>20 %), while the PDR in layer A is as small as 6 %. The mean lidar ratios at 355 (S_{355}) and 532 nm (S_{532}) were nearly same within the standard deviations: 48.6(±8.5) and 43.1(±7.0) sr, respectively in the dust-like layer (3.5-4.3 km). The value of PDR and S_{532} is similar to our previous observations.[3,18] The value of S_{355} is close to the lidar ratio observed for Saharan dust at 351 nm in southern Italy (~50 sr)[19], but smaller than what was observed in Leipzig, Germany (50-80 sr).[10] Mattis et al. also found that S_{355} is 10-30 % higher than S_{532}.[10] The difference in the lidar ratio values might be attributed to differences in shape, size or absorption properties of mineral particles.

In addition, we can see interesting differences of aerosol optical properties besides the large difference of the PDR in the layers A and B; a higher BAE in layer A (~1.2) than in layer B (~0.3) in Fig. 3, which suggests that layer A might be composed of finer aerosols. Since the relative humidity in the layers A and B are nearly identical (~40 %) as shown in Fig. 3, we can reject the assumption that hygroscopic growth of mineral dust reduces the depolarization ratio.

3.2.Case of Siberian forest-fire smoke

In the spring and summer of 2003, an unusually high number of forest fires occurred in Siberia.[11] Smoke plumes originating from these fires were transported over Japan with westerly wind. Fig. 4 shows a time-height plot of the backscatter coefficient and the total depolarization ratio at 532 nm on 21 May 2003. A high aerosol optical depth (τ_a) at the wavelength (λ) of 500 nm of more than 2.0 was observed in the daytime by collocated Sun photometer. The back trajectory analyses show that the airmass from 2 to 4 km trace back to regions of intense forest-fire from the west of Lake Baykal to the east of the border of China, Russia and Mongolia. The smoke layer sharply dropped off at ~4 km. The upper part (3-4 km) of the smoke layer showed a depolarization ratio of about 6 %. A similar feature was also observed in Suwon (37.14° N, 127.04° E), Korea.[20]

Fig. 5 shows the mean profiles of optical properties for a measurement from 1040 to 1349 UTC. A prominent layer between 2.5 and 4 km shows different optical properties separated at the peak (~3.2 km) from the intensive parameters, i.e., S_{532}, PDR, and AE. The upper part except the rim had the following features: i) BAE is high (~1.9) while AE is small (~0.7), ii) S_{532} (~65 sr) is apparently higher than S_{355} (~40 sr), iii) PDR (~6 %) is higher than that in the

lower part. On the other hand, in the lower part, S_{532} and PDR drop to ~40 sr and ~3 %, respectively, while AE increases to be ~1.2.

The relationship between S_{355} and S_{532}, i.e., $S_{532}>S_{355}$, is consistent with the observation over central Europe of aged smoke from Canada during the Lindenberg Aerosol Characterization Experiment LACE98.[21] A part of this Siberian smoke was also detected over central Europe and confirmed the same relationship between S_{355} and S_{532}.[11] The non-zero depolarization ratio might be caused by soil material that was uplifted into the forest fire plume[22], or the nonsphericity of the particles due to coagulation of smoke particles.[23] The latter explanation sounds more presumable because no signature of mineral dust was found by a chemical analysis of aerosols sampled at the summit of Mt. Fuji (3,776 m above sea level and ~100 km west from Tokyo) in the same period.[24]

The relatively small AE (~0.7) in the wavelength range from 355-532 nm for the smoke layer is supported by the evidence observed by Sun/sky photometer for cases of heavy smoke events in South America and South Africa[25]: a significant positive curvature in the $\log(\tau_a)$ versus $\log(\lambda)$ relationship, and in fact the analysis of the collocated TUMSAT skyradiometer (POM-01, Prede) also shows such relationship in the daytime.

4. DISCUSSIONS

4.1. Microphysical properties of the smoke aerosol retrieved from inversion

We applied the method of inversion with regularization only for the case of smoke to retrieve the microphysical properties using the backscatter coefficients at 355, 532, 1064 nm and the extinction coefficients at 355 and 532 nm.[9,21,26] We cannot apply currently the inversion code for Asian dust case which poses a high PDR, i.e., nonsphericity, because the inversion strongly relay on the assumption of spherical (Mie) particles. We found 0.22(±0.04) μm for the effective (surface-area mean) radius and 0.95(±0.06) for the single scattering albedo (SSA) at 532 nm around the peak of the smoke layer. Fig. 6 shows effective radius and single scattering albedo for selected height ranges. Comparison between a typical column-integrated volume size distribution derived from the skyradiometer[27] and that from the present inversion is indicated in Fig. 7. The results indicate that particles in the accumulation mode are dominant, which is a typical feature for this kind of aerosols. The relatively high SSA indicates low absorbing particles. It should be worthwhile to mention that the larger effective radius of 0.35(±0.07) μm with similar SSA of 0.97(±0.04) was retrieved with the same inversion code for the hemispheric transported smoke over Leipzig, Germany on May 29, 2003, which suggests the evolvement of the smoke aerosols.[28]

In comparison, we mention that the typical mean radius and the SSA of Asian dust plumes obtained by intensive airborne in situ measurements during the ACE-Asia are 2-3 μm and 0.96(±0.01) at 550 nm, respectively.[3,29]

4.2.Estimation of aerosol direct radiative forcing for the smoke case

There are relatively few literatures which presents the radiative forcing calculations using lidar data.[22,30,31] Here we attempted to estimate the aerosol direct radiative forcing (ADRF) for the smoke case on 21 May 2003 base on the extinction coefficient profile from the lidar measurement at 532 nm and microphysical properties derived from the inversion. We used the radaitive transfer code FSTAR5C.[33] We estimated the ADRF in the shortwave radiation (0.2-4.0 μm) by assuming the flowing constant atmospheric condition; the temperature, pressure, relative humidity profiles from the radiosonde data at Tateno, 12 UTC. Daily mean ADRF is thus evaluated as –39 and –51 W/m^2 at the top of the atmosphere and the surface, respectively. Since we used wavelength independent refractive indices of particles from the inversion, we also calculated the ADRF using the column-averaged size distribution and

refractive indices (wavelength dependent) retrieved from the skyradiometer analysis in the daytime. We found that both values agree each other if the mean refractive index is similar. The daily mean heating rate due to the aerosols is also obtained, which maximum reaches ~0.7 K per day just above the peak of the aerosol extinction profile.

5. CONCLUSIONS AND SUMMARY

The distinct optical signatures for mineral dust and aged smoke presented here well demonstrate how multi-wavelength Raman lidar including a depolarization channel is useful to characterize tropospheric aerosols resolving with height; for the Asian dust case we found a high PDR at 532 nm over 20 % and a small wavelength dependence of the lidar ratio between 355 and 532 nm (43-49 sr), for the smoke case we found that a small PDR of 5-8 % or less and a high wavelength dependence of the lidar ratio: S_{355} is ~40 sr, while S_{532} is ~65 sr. We successfully derived the climate-relevant microphysical parameters, e.g. effective radius and single scattering albedo, for the smoke case using the inversion code. We also attempted to evaluate the aerosol radiative forcing based on the height-resolved parameters using the radiative transfer code. Such an advanced Raman lidar is especially useful for the characterization of the complex aerosols found over East Asia and has a potential for application in global aerosol lidar networking in future.

ACKNOWLEDGEMENTS

This work is supported by Grand-in-Aid for Scientific Research on Priority Areas under Grant No. 14048232 from the Ministry of Education, Culture, Sports, Science and Technology, and Global Environment Research Fund for the project "Study of the dynamic transport mechanism and environmental effect of Kosa aerosol originated from the northern Chinese areas", from the Ministry of the Environment. We also acknowledge partial supports from the projects "Variability of Marine Aerosol Properties (VMAP)" and "Asian Atmospheric particle Environment Change Studies (APEX)" of CREST of Japan Science and Technology Agency, and the joint research programs of CEReS, Chiba University (14-5), (15-7) and (16-4).

REFERENCES

1. IPCC (The Intergovernmental Panel on Climate Change), *Climate Change 2001: The Scientific Basis*, 896 pp., Cambridge Univ. Press, 2001.
2. B. J. Huebert et al., "An overview of ACE-Asia: Strategies for quantifying the relationship between Asian aerosols and their climate impacts", *J. Geophys. Res., 108(D23)*, 8633, doi:10.1029/2003JD003550, 2003.
3. T. Murayama et al., "An intercomparison of lidar-derived aerosol optical properties with airborne measurements near Tokyo during ACE-Asia", *J. Geophys. Res., 108(D23)*, 8651, doi:10.1029/ 2002JD003259, 2003.
4. T. Murayama, "Formation of ice cloud from Asian-dust particles in the upper troposphere", *Proc. 4153*, pp.218-225, 2001.
5. T. Murayama et al., "Ground-based network observation of Asian dust events of April 1998 in east Asia", *J. Geophys. Res., 106(D16)*, pp.18,345-18,359, 2001.
6. K. Sassen, "Indirect climate forcing over the western US from Asian dust storms", *Geophys. Res. Lett., 29(10)*, 1465, doi:10.1029/2001GL014051, 2002.
7. K. Sassen, P. J. DeMott, J. M. Prospero, M. R. Poellot, "Saharan dust storms and indirect aerosol effects on clouds: CRYSTAL-FACE results", *Geophys. Res. Lett., 30 (12)*, 1633, doi:10.1029/2003GL017371, 2003.

8. T. Sakai, T. Nagai, M. Nakazato, and T. Matsumura, "Raman lidar measurement of water vapor and ice clouds associated with Asian dust layer over Tsukuba, Japan", *Geophys. Res. Lett., 31*, L06128, doi:10.1029/2003GL019332, 2004.
9. D. Müller et al., "Comprehensive particle characterization from three-wavelength Raman-lidar observations: case study", *Appl. Opt., 40*, pp.4863-4869, 2001.
10. I. Mattis et al., "Dual-wavelength Raman lidar observations of the extinction-to-backscatter ratio of Saharan dust", *Geophys. Res. Lett., 29*, doi:10.1029/2002GL014721, 2002.
11. I. Mattis et al., "Unexpectedly high aerosol load in the free troposphere over central Europe in spring/summer 2003", *Geophys. Res. Lett., 30*, 2178, doi:10.1029/2003GL018442, 2003.
12. T. Murayama et al., "Application of lidar depolarization measurement in the atmospheric boundary layer: Effects of dust and sea-salt particles", *J. Geophys. Res., 104(D24)*, pp.31,781-31,792, 1999.
13. T. Murayama, D. Müller, K. Wada, A. Shimizu, M. Sekiguchi and T. Tsukamoto, "Characterization of Asian dust and Siberian smoke with multi-wavelength Raman lidar over Tokyo, Japan in spring 2003", *Geophys. Res. Lett., 31, L23103*, doi:10.1029/2004GL021105, 2004.
14. A. Ansmann et al., "Combined Raman elastic -backscatter LIDAR for vertical profiling of moisture, aerosol extinction, backscatter, and lidar ratio", *Appl. Phys., B55*, pp.18-28, 1992.
15. D. N. Whiteman, S. H. Melfi, and R. A. Ferrare, "Raman lidar system for the measurement of water vapor and aerosols in the Earth's atmosphere", *Appl. Opt, 31*, pp.3068-3082, 1992.
16. D. N. Whiteman, "Examination of the traditional Raman lidar technique. I. Evaluating the temperature-dependent lidar equations", *Appl. Opt., 42*, pp.2571-2593, 2003.
17. F. G. Fernald, "Analysis of atmospheric lidar observations: some comments", *Appl. Opt., 23*, pp.652-653, 1984.
18. T. Murayama, "Optical properties of Asian dust aerosol lofted over Tokyo observed by Raman lidar", in *Lidar Remote Sensing in Atmospheric and Earth Sciences (Proceedings of the 21th ILRC)*, edited by L. R. Bissonnette, G. Roy, and G. Vallée, pp.331-334, Defense R&D Canada – Valcartier, Québec, 2002.
19. F. De Tomasi, A. Blanco and M. R. Perrone, "Raman lidar monitoring of extinction and backscattering of African dust layers and dust characterization", *App. Opt., 42*, pp.1699-1709, 2003.
20. C. H. Lee et al., "Continuous measurements of smoke of Russian forest fire by 532/1064 nm Mie scattering Lidar at Suwon, Korea", in *Reviewed and Revised Papers presented at the 22nd International Laser Radar Conference*, G. Papparado and A. Amodeo Editors, *ESA SP-561*, pp.535-538, 2004.
21. U. Wandinger et al., "Optical and microphysical characterization of biomass-burning and industrial-pollution aerosols from multiwavelength lidar and aircraft measurements", *J. Geophys. Res., 107(D21)*, 8125, doi:10.1029/ 2000JD000202, 2002.
22. M. Fiebig et al., "Optical closure for an aerosol column: Method, accuracy, and inferable properties applied to a biomass-burning aerosol and its radiative forcing", *J. Geophys. Res., 107(D21)*, 8130, doi:10.1029/2000JD000192, 2002.
23. J. V. Martins et al., "Sphericity and morphology of smoke particles from biomass burning in Brazil", *J. Geophys. Res., 103(D24)*, pp.32051-32057, 1998.
24. N. Kaneyasu, National Institute of Advanced Industrial Science and Technology, *private communication*, 2004.

25. T. F. Eck et al., "Wavelength dependence of the optical depth of biomass burning, urban, and desert dust aerosols", *J. Geophys. Res., 104(D24),* pp.31,333-31,349, 1999.
26. I. Veselovskii et al., "Inversion with regularization for the retrieval of tropospheric aerosol parameters from multiwavelength lidar sounding", *Appl. Opt., 41*, pp.3685-3699, 2002.
27. T. Nakajima et al., "Use of sky brightness measurements from ground for remote sensing of particulate polydispersions", *Appl. Opt., 35*, pp.2672-2686, 1996.
28. I. Mattis et al., "Siberian forest-fire smoke observed over central Europe in spring/summer 2003 in the framework of EARLINET", in *Reviewed and Revised Papers presented at the 22nd International Laser Radar Conference*, G. Papparado and A. Amodeo Editors, *ESA SP-561*, pp.857-860, 2004.
29. T. L. Anderson et al., "Variability of aerosol optical properties derived from in situ aircraft measurements during ACE-Asia", *J. Gephys. Res., 108(D23)*, 8647, doi:10.1029/2002JD003247.
30. J. Redemann et al., "Case studies of the vertical structure of the direct shortwave aerosol radiative forcing during TARFOX", *J. Geophys. Res., 105(D8)*, pp.9971-9979, 2000.
31. J. G. Won et al., "Estimation of direct radiative forcing of Asian dust aerosols with Sun/sky radiometer and lidar measurements at Gosan, Korea", *J. Metorol. Soc. Jpn., 82, 1*, pp.115-130, 2004.
32. T. Y. Nakajima, T. Nakajima, T. Aoki, A. Higurashi, A. Tanaka, M. M. Verstraete, Y. Hashibe, *GSS Reference Hand book (Rstar Reference Handbook), JAXA EORC Bulletin, 15*, 2004.

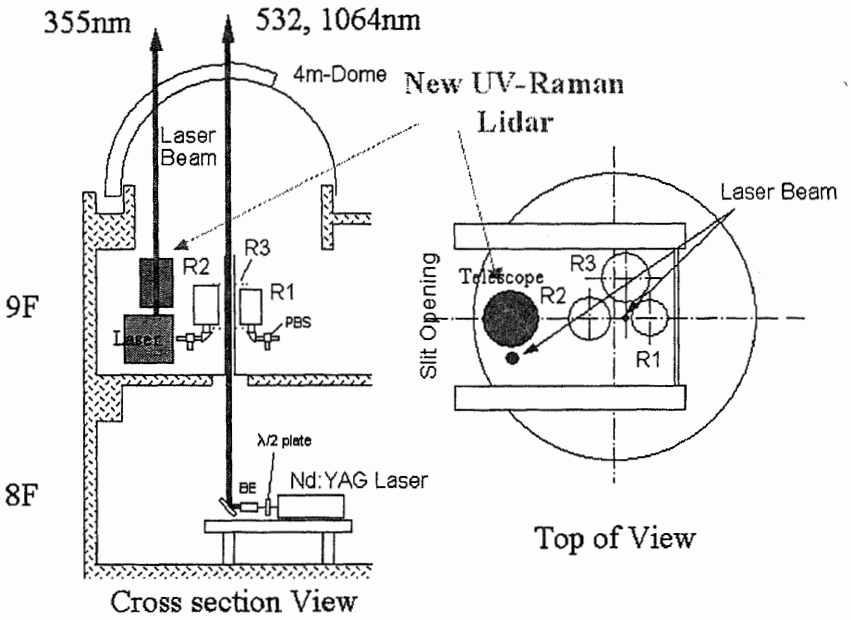

Fig. 1. Schematic view of the TUMSAT multi-wavelength Raman lidar system.

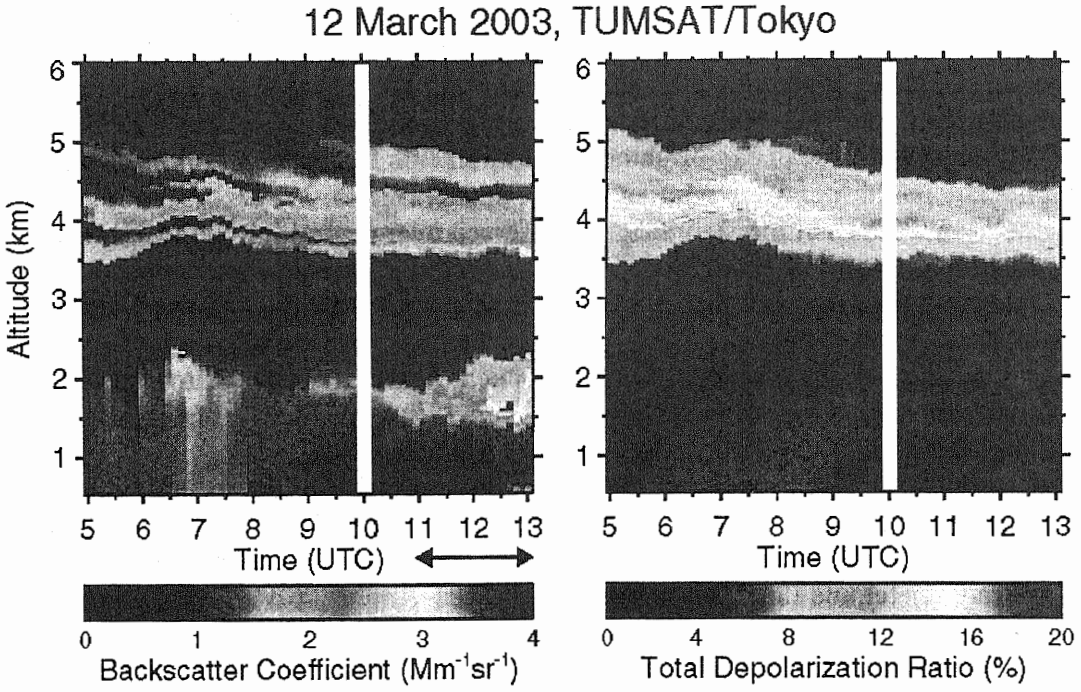

Fig. 2. Time-height cross section of aerosol backscatter coefficients and total depolarization ratio at 532 nm over TUMSAT in Tokyo, Japan on 12 March 2003.[13]

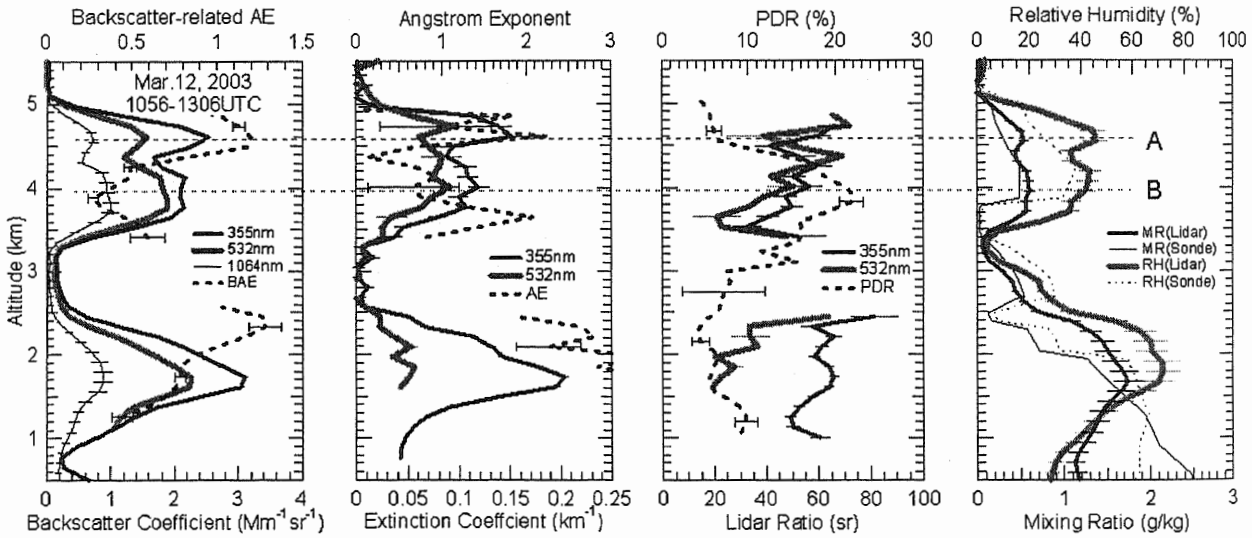

Fig. 3. Mean profiles of aerosol optical properties and water-vapor mixing ratio for the measurement from 1056 to 1306 UTC on 12 March 2003.[13] BAE and AE denote Backscatter-related Ångström Exponent and Ångström Exponent for the extinction coefficient between 355 and 532 nm, respectively. The mixing ratio and relative humidity obtained from radiosonde at Tateno (12 UTC) are shown for reference.

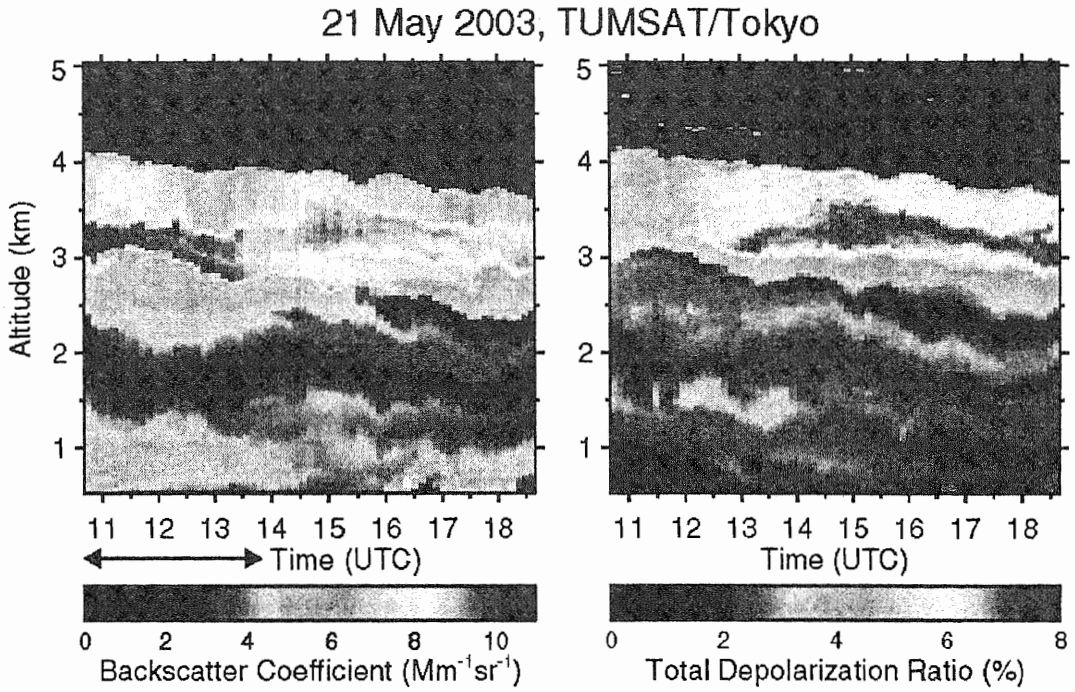

Fig. 4. As in Fig. 2, except for 21 May 2003.[13]

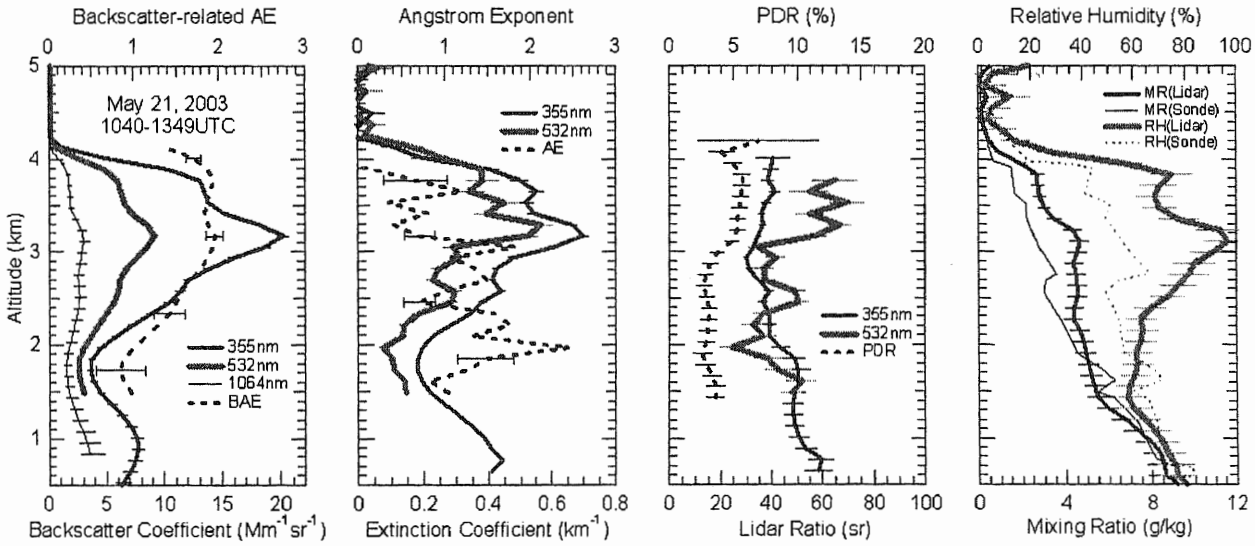

Fig. 5. As in Fig. 3, except for the period from 1040 to 1349 UTC on 21 May 2003.[13]

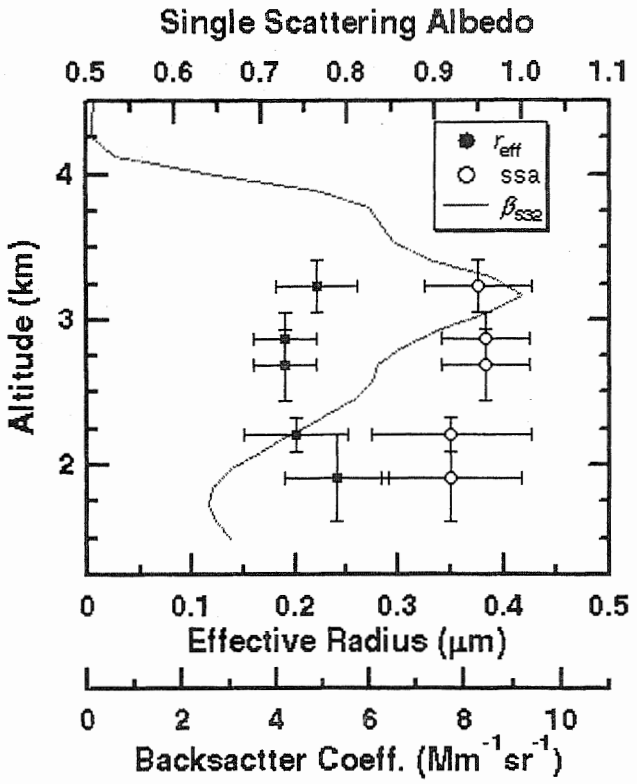

Fig. 6. Vertical variation of the effective radius and single scattering albedo at 532 nm retrieved from the Raman lidar observation shown in Fig. 5.[13]

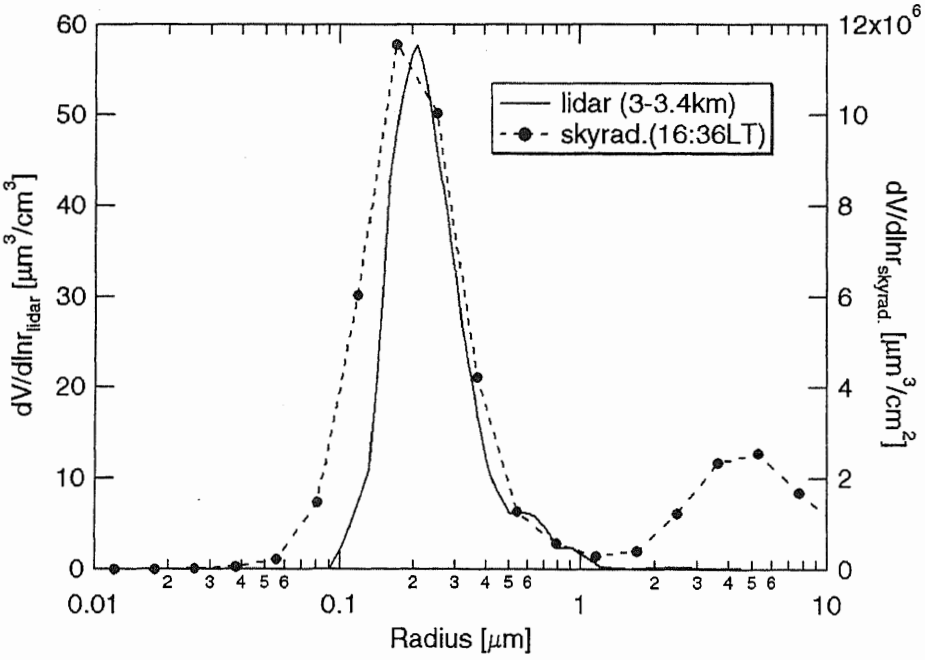

Fig. 7. Comparison between the volume size distributions retrieved from the Raman-lidar and skyradiometer inversions on 21 May 2003.